I

Imaging and modelling of fungi in the environment

1

Imaging complex nutrient dynamics in mycelial networks

DANIEL P. BEBBER[1], MONIKA TLALKA[1], JULIET HYNES[2], PETER R. DARRAH[1], ANNE ASHFORD[3], SARAH C. WATKINSON[1], LYNNE BODDY[2] AND MARK D. FRICKER[1]

[1]*Department of Plant Sciences, University of Oxford*
[2]*Cardiff School of Biosciences, Cardiff University*
[3]*School of Biological, Earth and Environmental Sciences, The University of New South Wales*

Introduction

Basidiomycetes are the major agents of decomposition and nutrient cycling in forest ecosystems, occurring as both saprotrophs and mycorrhizal symbionts (Boddy & Watkinson, 1995; Smith & Read, 1997). The mycelium can scavenge and sequester nutrients from soil, concentrate nutrients from decomposing organic matter, relocate nutrients between different organic resources, and ultimately make nutrients available to plants to maintain primary productivity. Hyphae of both saprotrophic and ectomycorrhizal basidiomycetes that ramify through soil often aggregate to form rapidly extending, persistent, specialized high-conductivity channels termed cords (Rayner *et al*., 1994, 1999; Boddy, 1999; Watkinson, 1999; Cairney, 2005). These cords form complex networks that can extend for metres or hectares in the natural environment. The distribution of resources is extremely heterogeneous and unpredictable in space and time, and these fungi have developed species-specific strategies to search for new resources and to capitalize on resources landing on their mycelial systems (Chapter 6, this volume). Thus the architecture of the network is not static, but is continuously reconfigured in response to local nutritional or environmental cues, damage or predation, through a combination of growth, branching, fusion or regression (Boddy, 1999; Watkinson, 1999; Chapter 6, this volume). At this stage it is not clear whether specific global mechanisms exist to couple local sensory perception and responses over different length scales specifically to maximize the long-term success of the whole colony, or whether such collective behaviour is an emergent property arising solely from local interactions of individual hyphae.

Fungi in the Environment, ed. G. M. Gadd, S. C. Watkinson & P. S. Dyer. Published by Cambridge University Press.

Embedded within the physical structure is an equally complex set of physiological processes that contribute to uptake, storage and redistribution of nutrients throughout the network in an apparently well coordinated manner (Olsson, 1999; Cairney, 2005). As the colony grows out from a resource base, nutrient translocation would be expected to be predominantly towards the growing margin. If additional resources are found, then re-distribution back to the base can also occur, although not necessarily by the same transport system at the same time. However, we know little about the cellular and sub-cellular anatomy of the pathway, the mechanism of transport and its driving forces, and the nature of the information pathways through mycelium that might contribute to coordinated system-wide responses to localized nutritional stimuli (Cairney, 2005; Watkinson *et al.*, 2006). A detailed understanding of nutrient translocation requires analysis of processes occurring across a range of length scales, from uptake by transporters in individual hyphae, to translocation through corded networks spanning several metres. In this chapter we describe the range of overlapping techniques that we are developing to try to track nutrient flow directly or indirectly in these systems across a range of length scales.

To simplify the initial state of the system, we have chosen to focus on microcosms in which foraging fungi grow from a central resource (agar or wood-block inoculum) over an inert (scintillation screen) or nutrient-depleted (sand or soil–sand mix) surface. Under these conditions, all nutrient transport, and in the first case water movement, is initially from the centre.

Transport at the micrometre to millimetre scale

The precise mechanisms underlying nutrient translocation in fungi are not yet known but are thought to include mass flow, diffusion, generalized cytoplasmic streaming and specific vesicular transport (Cairney, 2005). It has been proposed that the highly dynamic pleiomorphic vacuolar system present in filamentous fungi of all the major fungal taxonomic groups so far examined might have a role in long-distance translocation over millimetres or centimetres (Ashford & Allaway, 2002). The structure of the vacuole within a single hypha develops from a complex reticulum of fine tubes interspersed with small spherical vacuoles at the tip (Fig. 1.1D) to a series of larger, more spherical, adherent vacuoles interconnected with fine tubes (Fig. 1.1A). As there are no convenient fluorescent probes to study N-movement directly, we have adopted an indirect approach to address whether the vacuolar system plays a role in long-distance transport of N. The lumen of the vacuole

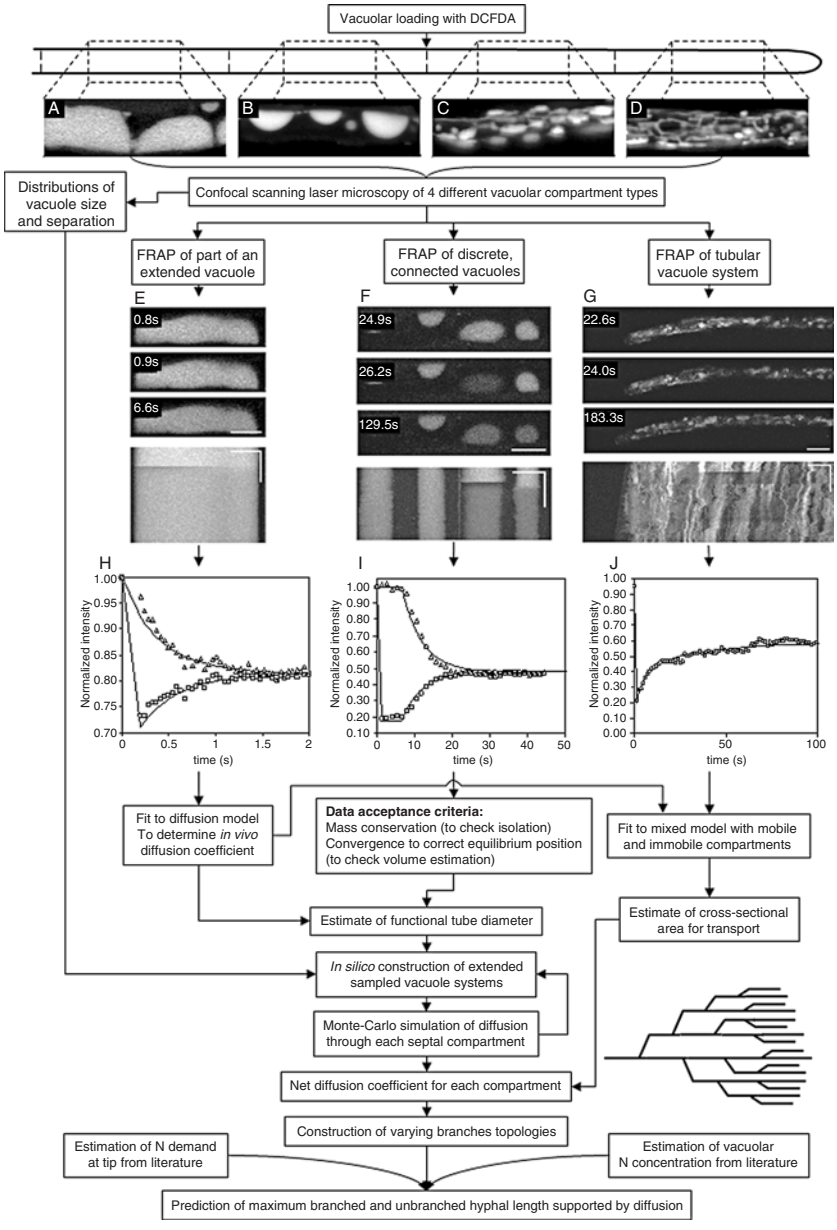

Fig. 1.1. Measurement and modelling of longitudinal vacuolar transport in *Phanerochaete velutina*. Vacuoles were labelled with carboxy-DFFDA (carboxydifluorofluorescein diacetate) and imaged with time-lapse confocal laser scanning microscopy in different septal compartments progressing towards the tip (A–D). Fluorescence recovery after photobleaching (FRAP) of part of single, isolated large vacuoles was used to determine the

can be labelled with fluorescent dyes, such as Oregon Green, which therefore provide a non-specific marker for any movement of the lumenal contents. The rate of movement can be determined in very small sections of individual hyphae by using fluorescence recovery after photobleaching (FRAP). In essence, a brief, high-intensity pulse of illumination is used to photobleach the fluorescent dye. The rate of recovery of signal following this bleaching gives a measure of the rate of movement from adjacent parts of the vacuole system and can be quantified. The following steps outline the protocol we have developed to build a complete model of vacuolar transport (Darrah *et al.*, 2006). A flow diagram is given in Fig. 1.1.

The vacuolar diffusion coefficient (D_v) of Oregon Green (OG) *in vivo* was estimated by FRAP of half a large, isolated vacuole by using rapid confocal imaging (Fig. 1.1E, H). Values measured *in vivo* compared favourably with theoretical and experimental values for fluorescein in pure water (deBeer *et al.*, 1997) suggesting that OG was freely diffusible in a largely aqueous vacuole. With a known value of D_v, it was possible to estimate the functional tube diameter *in vivo* between two vacuoles of defined size and separation by using FRAP and assuming dye movement was mediated only by diffusion (Fig. 1.1F). In instances where the only connection was between the vacuoles under investigation and not adjacent neighbours, a diffusion model described the data well (Fig. 1.1I). Functional tube diameters determined *in vivo* compared well with estimates from EM data of 0.24–0.48 μm (Rees *et al.*, 1994) and 0.3 μm (Uetake *et al.*, 2002). To estimate the transport characteristics of an entire septal compartment, the values of D_v and the median tube diameter were combined with measured distributions of vacuole length, width and separation to construct an *in silico* vacuole system for each septal compartment. The resulting model was run with constant boundary conditions of $C = 0$ and $C = 1$ at the two ends of the filament and the steady-state flux recorded, which

Fig 1.1. (cont.)
vacuolar diffusion coefficient for Oregon Green *in vivo* (E, H); the tube diameter between two connected vacuoles (F, I); and the effective diffusion coefficient for the tubular vacuolar region at the tip (G, J). These data were combined with samples of the vacuolar morphology from each compartment type to construct an *in silico* model of the vacuolar system. The net diffusion coefficient was determined for each compartment by Monte Carlo simulation. The maximum hyphal length that could be supported by diffusion was then calculated by using estimates of the N demand at the tip and the maximum likely vacuolar N concentration. Horizontal scale bar, 10 μm. Vertical scale bar, 2 s (E) or 60 s (F, G).

allowed an effective diffusion coefficient, $D_v\alpha$, for the whole compartment to be calculated from Fick's first law, where α has a range from 0–1 and measures the reduction in the vacuolar diffusion coefficient D_v caused by including many vacuoles and tubes of smaller diameter in the string relative to a uniform vacuole of the same length. One thousand Monte Carlo simulations of *in silico* hyphae were conducted to give a mean α for this compartment type. Similar simulations were run for two other categories of vacuolar organization with progressively smaller vacuoles and increasing amounts of tubular network (Darrah *et al.*, 2006).

In contrast to the discrete vacuoles distal from the tip, the tubular vacuole region consisted of a structurally complex reticulate network of predominantly longitudinal, tube-like elements and small vesicles (Fig. 1.1D). Superficially the network appeared quite dynamic, but most of the motion appeared to be short-range micrometre-scale oscillations rather than longer-range translocation of entire structures. Net diffusion in this tubular region was determined by FRAP of a region 40–60 μm long spanning the entire hyphal diameter (Fig. 1.1G). The data were well described by a model that included a well-connected (tubular) component and a smaller immobile (vesicle) phase (Fig. 1.1J).

Diffusion was a sufficient mechanism to explain observed transport in the various regions of the vacuolar organelle. Therefore, we used Fick's first law to estimate the length scales for effective diffusional translocation to maintain tip growth through the system at steady state with literature-based estimates of the concentration gradient for N in the vacuole system, a value for the N demand at the tip, and the effective diffusion coefficient, D_e, for the composite branched structure. This last value was calculated from the composite diffusion coefficients for each type of compartment. Although this analysis is not yet complete, preliminary observations suggest that an unbranched hypha possessing a continuous tubular vacuole system could sustain growth over a transport distance of around 12–24 mm. Conversely, diffusion alone in a maximally branched system would operate over only a few millimetres. This poise between translocation being sufficient or insufficient depending on the amount of branching and status of the vacuolar network suggests that the vacuolar system is an important organ for coordinating and controlling tip growth and branching. For example, the range of simulated effective diffusion coefficients varied by orders of magnitude when we used the sampled vacuole distribution data. It is therefore possible that the vacuolar system could be regulated to change its translocation capacity according to local nutrient conditions. The system could thus shift between increasing transport to

tips or preventing unnecessary nutrient mobility by isolating tips. An alternative possibility is that the vacuolar system translocates material acquired by the tips back into the main colony, against the mass flow component needed for tip growth (Darrah *et al.*, 2006).

Transport at the millimetre to centimetre scale

One approach to measuring transport of solutes is to follow the movement of radiolabelled compounds through the mycelium. Typically, the final radiolabel distribution has been visualized by using autoradiography techniques or phosphor-imaging, or analysed by destructive harvesting of the tissues followed by scintillation counting. We have developed a novel non-invasive technique to track movement of ^{14}C-labelled N compounds in foraging mycelial networks in contact with an inert scintillation screen, by using photon-counting scintillation imaging (PCSI) (Tlalka *et al.*, 2002). We have developed two protocols to analyse the distribution patterns of the non-metabolized amino-acid analogue α-amino-isobutyrate (^{14}C-AIB). The first approach focuses on the correlation between local distribution patterns of AIB and local patterns of growth and is designed to accommodate the marked asymmetry in colony development, particularly in the presence of additional resources that provide a highly polarized resource environment. The second approach focuses on mapping the pulsatile component of transport that was observed superimposed on the net AIB translocation pattern (Tlalka *et al.*, 2002, 2003).

In simple microcosms with mycelium growing out from a central inoculum, ^{14}C-AIB was taken up and distributed through the growing colony. The AIB distribution pattern can be characterized by three parameters, the position of the centre of mass of AIB ($CM_{\Delta AIB}$) relative to the centre of the inoculum, the extent to which the AIB was spread evenly around the colony or concentrated in a particular area (measured by the angular concentration of the AIB, $Conc_{\Delta AIB}$) and the alignment of the $CM_{\Delta AIB}$ vector with the new resource, if present. We have no completely independent measure of colony growth during the experiment as (i) PCSI precludes separate bright-field imaging, and (ii) the lack of contrast between a white mycelium and a white screen on which it is growing makes it extremely difficult to characterize growth effectively. As an alternative approach, we determined the area covered from the scintillation image by using contrast-limited adaptive histogram equalization (CLAHE) and automated grey-scale thresholding algorithms (Otsu, 1979). We have validated this approach by comparison of the segmented boundary with a bright-field

image of a colony grown across Mylar film 1.5 µm thick to facilitate imaging against a black background at the end of the PCSI experiment (Fig. 1.2). There was very good correspondence between the automatically segmented area (Fig. 1.2A) and the visible distribution pattern of the colony (Fig. 1.2B). In a similar manner to the analysis of AIB distribution, we used difference values for the change in area, averaged over a sliding 12 or 24 h window, and calculated the displacement of the centre of mass of the change in area ($CM_{\Delta area}$), the angular concentration ($Conc_{\Delta area}$) and the alignment of the *Δarea* vector to quantify the dynamics of the underlying processes (Fig. 1.3). In the first phase of colony development, the change in area and transport were almost symmetrical (Fig. 1.3A, B). This was followed by a transition to sparser, more asymmetric growth. The duration of the first growth phase depended on nutrient availability and developmental age of the colony. The different growth phases can be described by two superimposed logistic equations, which allow normalization of all data sets to a common developmental stage of the colony.

Time series data for $CM_{\Delta AIB}$, $Conc_{\Delta AIB}$, $CM_{\Delta area}$ and $Conc_{\Delta area}$ were normalized to the start of the second growth phase and fitted by using

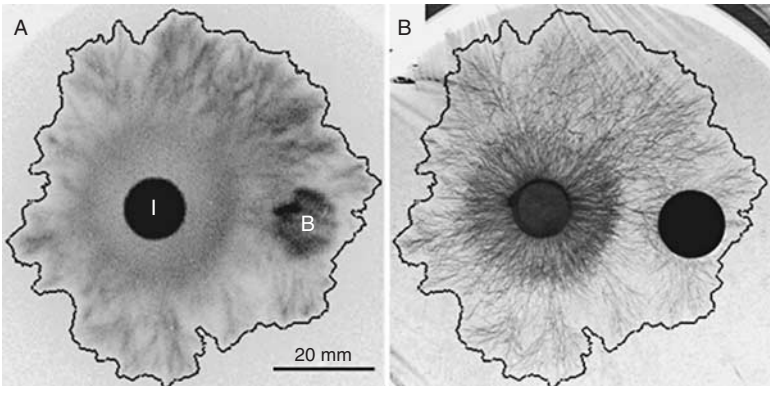

Fig. 1.2. Validation of automated colony area segmentation from photon-counting scintillation images. The area of a growing colony was estimated from photon-counting scintillation imaging (PCSI) by a combination of contrast-limited adaptive histogram equalization (CLAHE) and automated grey-scale segmentation. The perimeter determined by this approach is shown superimposed on the PCSI image (A) and the corresponding bright-field image (B) taken at the end of the experiment for a colony growing from an agar inoculum (I) with a filter-paper bait (B). The difference between the first phase of symmetrical growth and the second phase of sparser, more asymmetric growth is also clearly visible in these images.

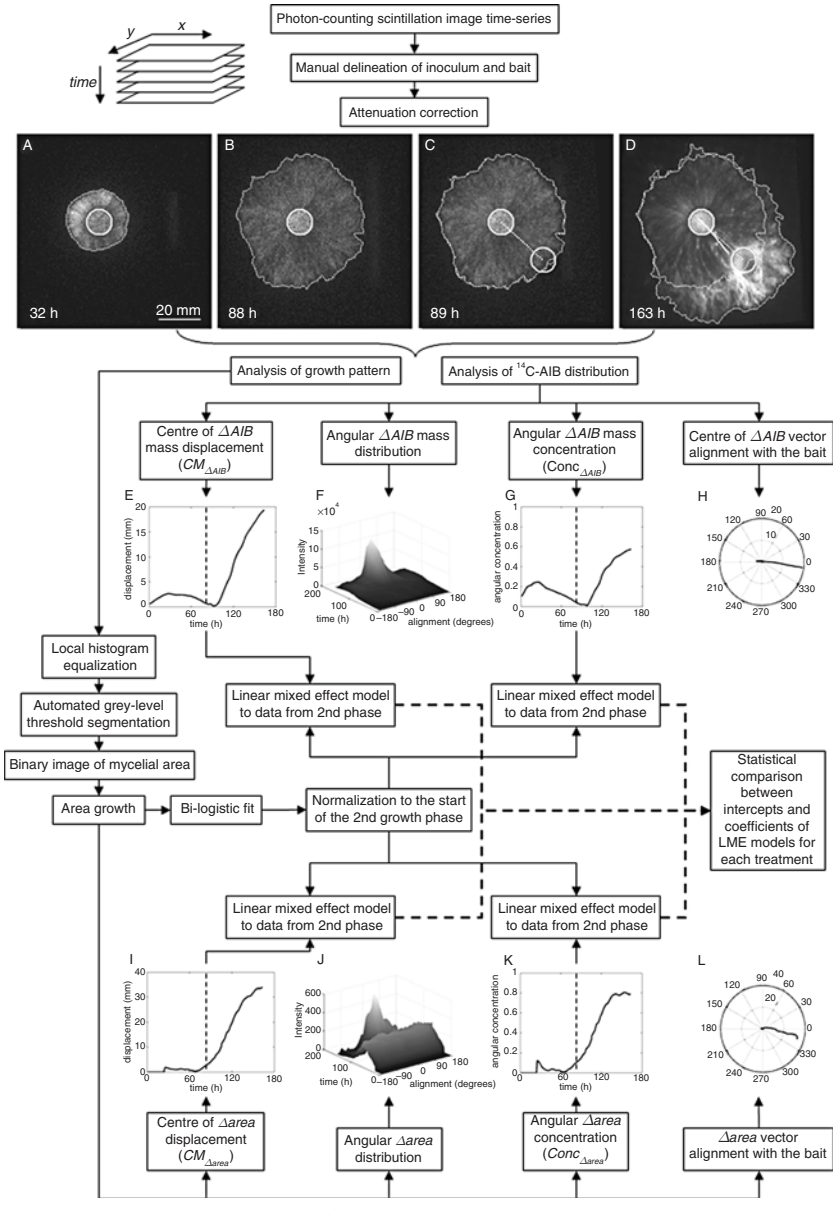

Fig. 1.3. Analysis of ^{14}C-AIB distribution and growth by using photon-counting scintillation imaging. Time-lapse photon-counting scintillation imaging (PCSI) was used to map the distribution of N in *Phanerochaete velutina* mycelium during growth from a central inoculum with or without the addition of either a glass-fibre or a filter-paper 'resource'. Representative PCSI images are shown (A–D) with the automatically

Linear Mixed Effects models (Pinheiro & Bates, 2000). Controls with no additions spontaneously switched to asymmetric growth and selectively allocated resources to broad sectors of the colony. Canalized flow patterns in cords also emerged with the transition to the second phase. Added damp cellulosic resources induced a change in internal nitrogen allocation, promoting marked N accumulation (Fig. 1.3E–G) and asymmetric growth (Fig. 1.3I–K) tightly focused on the new resource (Fig. 1.3H, L). The effect of a damp glass-fibre 'resource' was more variable, often with a transient response to perturbation that was not sustained in comparison with filter-paper resources.

Analysis of the pulsatile component

In addition to the evolution of the longer-term trends described above, a strong pulsatile component was found to be associated with rapid transport, particularly through corded systems (Tlalka *et al*., 2002, 2003). We have previously analysed this pulsatile component by using Fourier techniques from discrete regions of interest manually defined on the image (Tlalka *et al*., 2002, 2003). For example, results for three regions shown in Fig. 1.4A are given in Fig. 1.4B–E. This revealed that the assimilatory mycelium on the inoculum and the foraging mycelium both pulsed, but were out of phase with each other. To determine whether there were other

Fig. 1.3. (cont.)
segmented colony margin shown as a dotted line around the periphery. A filter-paper resource was added at 89 h (C) and resulted in localized increased transport of ^{14}C-AIB and localized growth (D). The magnitude of these effects was determined from analysis of the displacement of the centre of mass of AIB ($CM_{\Delta AIB}$, E) and displacement of the centre of mass of the colony area ($CM_{\Delta area}$, I), in which zero displacement represents symmetrical N distribution and growth. The displacement following resource addition ($CM_{\Delta AIB}$) is plotted as a solid line from the centre of the inoculum in (D). The total angular distribution in 12° sectors of AIB (F) and growth (J) indicates how tightly focused these changes were. The angular concentration ($Conc_{\Delta AIB}$ and $Conc_{\Delta area}$) provides a quantitative measure of these distributions (G, K), in which values of zero represent completely even distribution or growth and values approaching 1 indicate a very tightly focused distribution. The alignment between the centre of the mass displacement vector and the vector between the inoculum and bait provides a measure of the degree to which resource allocation is directed specifically towards the bait. A value of zero represents perfect alignment. Linear mixed effects models were fitted to the data for the $CM_{\Delta AIB}$, $CM_{\Delta area}$, $Conc_{\Delta AIB}$ and $Conc_{\Delta area}$ to allow statistical comparison between the control and the treatments.